PRAMANA — journal of physics

Vol. 79, No. 4
October 2012
pp. 757–780

Low-energy neutrino measurements

DAVIDE D'ANGELO
Università degli Studi di Milano e I.N.F.N. sez. di Milano-via Celoria, 16-20133 Milano, Italy
E-mail: davide.dangelo@mi.infn.it

Abstract. Low-energy solar neutrino detection plays a fundamental role in understanding both solar astrophysics and particle physics. After introducing the open questions on both fields, we review here the major results of the last two years and expectations for the near future from Borexino, Super-Kamiokande, SNO and KamLAND experiments as well as from upcoming (SNO+) and planned (LENA) experiments. Scintillator neutrino detectors are also powerful antineutrino detectors which can detect neutrinos emitted by the Earth crust and mantle. First measurements of geoneutrinos have occurred which can bring fundamental contribution in understanding the geophysics of the planet.

Keywords. Solar neutrinos; geoneutrinos; low-energy neutrinos; MSW-LMA; standard solar model.

PACS Nos 14.60.Pq; 26.65.+t; 96.60.Jw

1. Solar neutrinos

Solar neutrino physics lies at the crossing between stellar astrophysics and particle physics beyond the Standard Model of electroweak interactions. The Standard Solar Model (SSM) describes the thermonuclear processes in the core of the Sun and foresees the emission of neutrinos from different species belonging to two groups of reactions, the so-called *pp*-chain and CNO cycle. The expected spectrum can be seen in figure 1a.

The long-standing Solar Neutrino Problem, consisting of reduced neutrino fluxes detected on Earth by many experiments in comparison to the model previsions, was solved during the last decade with the establishment of the neutrino oscillation mechanism. Neutrinos, which are no longer believed to be massless, are emitted by the Sun as electron flavour leptons but propagate as mass eigenstates and arrive on Earth as a combination of different flavour eigenstates, to which detectors are differently sensitive. The phenomenon in which the oscillation is enhanced by resonance in the solar matter is known as the MSW effect [1]. A global analysis of solar and reactor neutrino observations indicates a best-fit point in the parameter space of the oscillation ($\Delta m^2 = 7.59 \pm 0.21 \cdot 10^{-5}$ eV^2, $\sin^2(2\theta_{12}) = 0.861^{+0.026}_{-0.022}$) [2] which is known as the large mixing angle (LMA) solution. The survival probability for electron flavour solar neutrinos as a function of energy as predicted in the MSW-LMA model is shown in figure 1b.

DOI: 10.1007/s12043-012-0385-3; ***e*Publication: 5 October 2012**

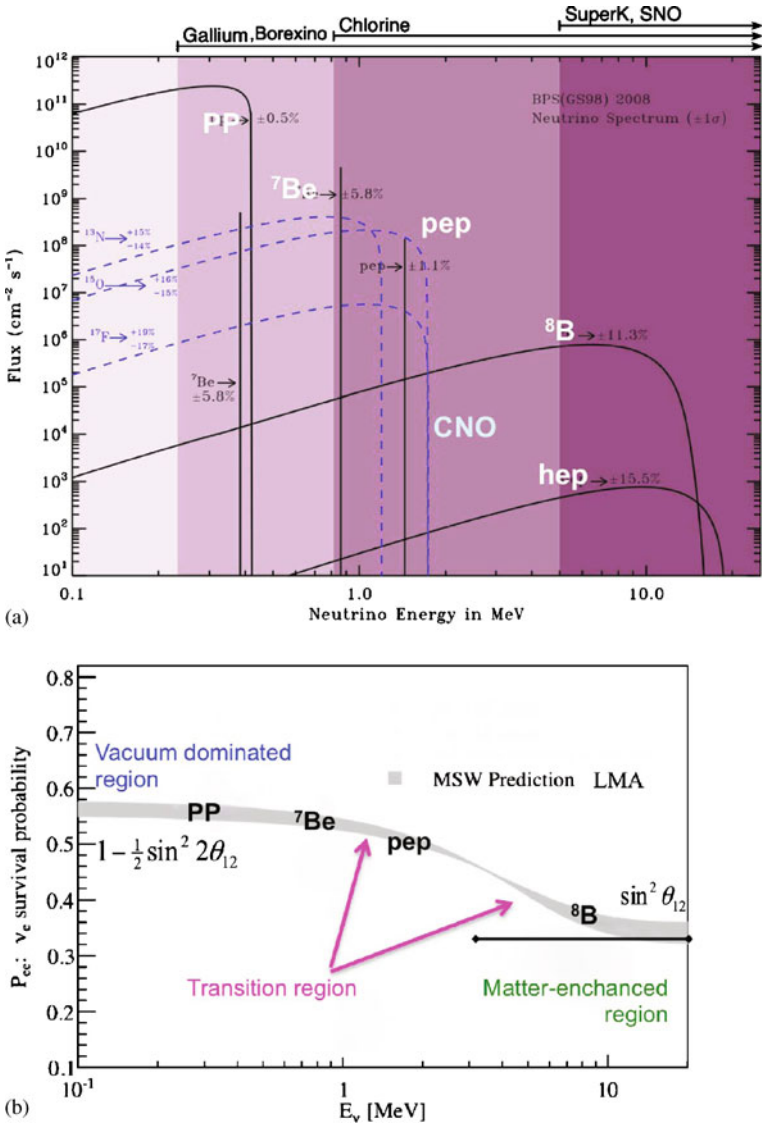

Figure 1. (**a**) Solar neutrino spectrum [4]. (**b**) Survival probability for solar electron neutrinos P_{ee} as predicted by the MSW-LMA model.

Actually, solar neutrino oscillation falls into a wider 3×3 oscillation scenario together with the atmospheric neutrino oscillation occurring between mass eigenstates 2 and 3. The complete parametrization is given by the PSMN mixing matrix, analogous to the quark mixing matrix [2]. The decoupling into two two-neutrino scenarios relies on the third mixing angle θ_{13} being null. This last hypothesis is being highly investigated in

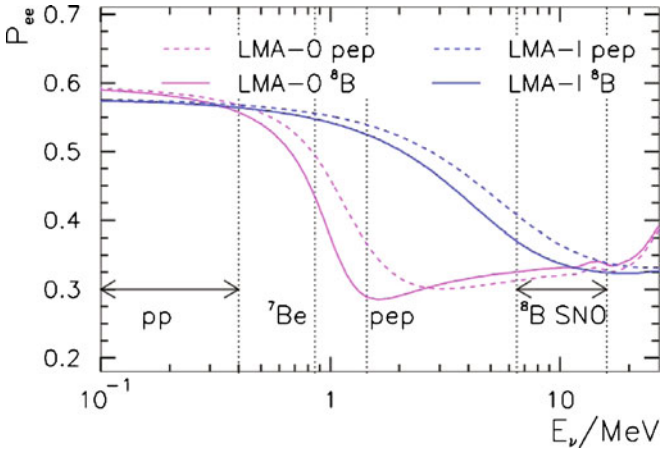

Figure 2. The non-standard interaction (NSI), labelled as LMA-0 predicts a different P_{ee} in the transition region with respect to LMA [5].

these years as moderate indications of non-zero values have recently appeared and would open up for the observation of CP violation in the leptonic sector [3].

1.1 *Open question in particle physics*

Neutrino physics has now entered the phase in which the precise determination of all oscillation parameters is crucial to unveil new physics. In the case of solar neutrinos, the LMA solution has been tested so far in the low-energy region (*pp* and ^{7}Be), the so-called vacuum-dominated regime with errors at the level of 10% or larger and in the high-energy region (^{8}B beyond 4–5 MeV), the matter-enhanced region; the intermediate transition region remains basically unexplored. A number of alternatives to MSW-LMA have been postulated over the years, the most popular one being non-standard neutrino interactions (NSI) [5]. The different survival probability shapes can be observed in figure 2. From the experimental point of view, there are multiple ways to shed light among the different models. The first step is reducing the error on the monochromatic emission of ^{7}Be at 862 keV which can also indirectly constrain the *pp* flux as this is so far only known from gallium radiochemical experiments [5a]. The detection of high-energy ^{8}B neutrinos started with Cherenkov detectors with a threshold of 7.5 MeV, which has recently been reduced to 3.5 MeV. Now scintillator detectors have lowered this threshold to 3 MeV and they are aiming to reach 2 MeV with the goal of observing the upturn of the survival probability foreseen by the LMA solution (figure 1b). Finally, a measurement of the *pep* monochromatic emission at 1.2 MeV will be a direct test of the transition region.

1.2 *Open question in solar physics*

At the same time, as the nature of neutrino is known more and more, neutrinos can play again the role of probes of the Sun's interior. In particular, the fundamental *pp*-neutrinos

are bound to the Sun light emission by the luminosity constraint [4]. However, the light takes $\sim 10^5$ yr to reach us, while neutrinos escape from the solar matter undisturbed. Consequently, a precision measurement of *pp*-neutrinos would test the stability of the Sun over this long time-scale. The SSM loosely predicts the contribution of the CNO cycle to the energy balance of the star to be $<1\%$ [4]. Detection of the so far unseen CNO neutrinos is therefore a major goal with important cosmological implications. Another open problem in solar modelling is the so-called 'solar metallicity puzzle'. Abundance of isotopes such as C, N, O, Ne and Ar is modelled starting from surface abundance measurements. The 'old' results, dated 1998 [6] and based on 1D modelling, have been improved with the help of 3D modelling (based on the same set of measurements) in 2005 and reviewed in 2009 [7] indicating the lower metallicity of the Sun. However, while the high-metallicity model is perfectly able to reproduce the sound speed profile in the Sun as determined by helio-seismological measurements, the low-metallicity model fails to match this constraint [8]. Models with different metallicities foresee different neutrino emissions, calling neutrino detectors for solving this ambiguity.

2. Recent results from solar neutrino experiments

There are four major experiments (figure 3) presently contributing to solar neutrino results and many being constructed or proposed. They rely on two complementary techniques: water Cherenkov for Super-Kamiokande and SNO, liquid scintillator for Borexino and KamLAND.

2.1 *Borexino*

Borexino is an organic liquid scintillator detector located in the underground Gran Sasso National Laboratory (LNGS) in central Italy under a limestone coverage of $\sim$1300 m ($\sim$3800 m w.e). Data taking started in 2007 which led to the first observation of the ^{7}Be monochromatic line.

2.1.1 *The detector.* The Borexino detector [9] is designed to have very low intrinsic background. The active target for this measurement is the inner detector (ID). Its central scintillation volume consists of 278 t of liquid scintillator, contained in a spherical,

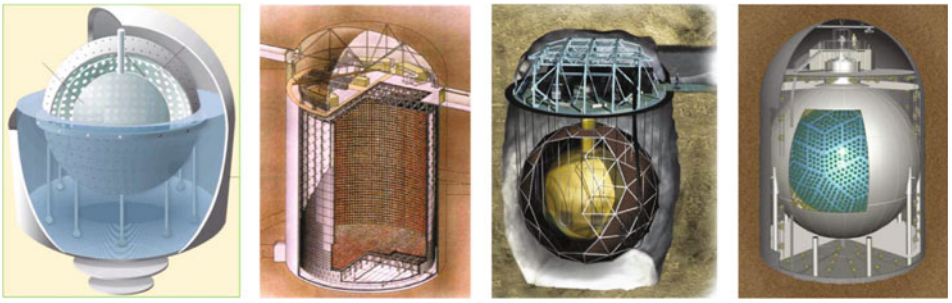

Figure 3. Sketches of principal solar neutrino detectors. From left to right: Borexino [9], Super-Kamiokande [10], SNO [11], KamLAND [12].

transparent, 8.5 m diameter, nylon inner vessel (IV). The surrounding 13.7-m-diameter stainless steel sphere (SSS) holds 2212 inward-facing 8″ photomultiplier tubes (PMT) for a 30% optical coverage. The ID is surrounded by a powerful muon outer detector (OD) [13], a high domed steel tank filled with 2 100 t of ultrapure water and instrumented with 208 PMTs which detect the muon Cherenkov emission.

2.1.2 *^{7}Be neutrino flux.* The radioactive decays of the remaining isotopes in the scintillator and in the surrounding detector's material cannot be disentangled on an event-by-event basis from neutrino interactions. Consequently, the neutrino flux is extracted from a fit to the energy spectrum, which accounts for all signal and background components (see figure 4). To limit the impact of external background, a fiducial volume is defined inside the IV via the reconstruction of the position of the events by fitting the arrival photon time distribution on the PMTs.

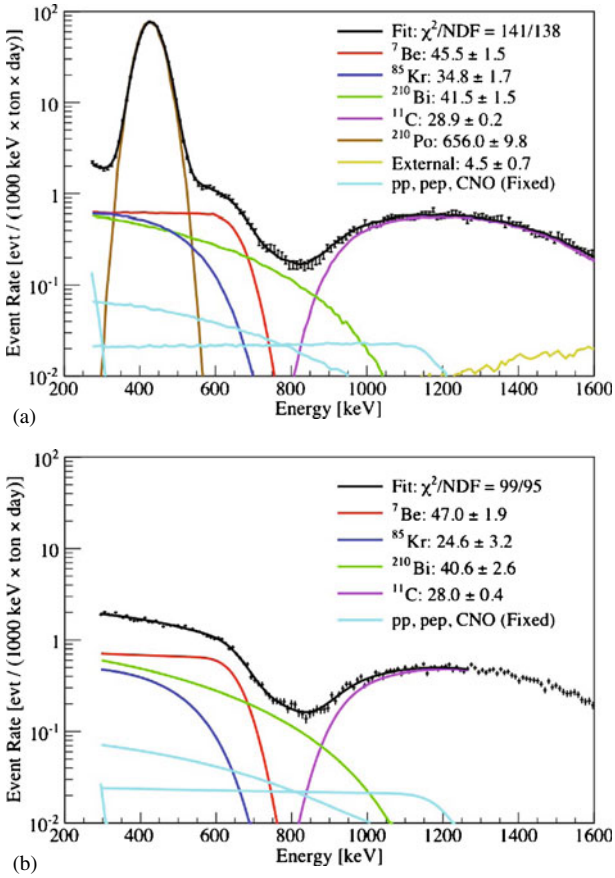

Figure 4. Borexino energy spectrum with (**a**) MC and (**b**) analytic fits for ^{7}Be analysis [15].

The first measurement of ^{7}Be neutrino flux came after only three months of data taking and was revised a year later with an error of 10% [14]. With the goal of reducing the systematic error, during the past two years the collaboration has performed a thorough set of calibration campaigns using α, β, γ and neutron sources deployed in different locations within the IV. The precise energy calibration of the detector up to about 2.5 MeV reduced the energy scale uncertainty to better than 1.5%; while the calibration of the position reconstruction algorithm allowed a determination of the fiducial volume to $-1.3\%/+0.5\%$. The spectral fit after 741 live days [15] is performed keeping the *pp*, *pep*, CNO and ^{8}B fluxes fixed to the values foreseen by the SSM (SP11 with High-Z), while the ^{7}Be flux and the backgrounds from ^{85}Kr(β^-), ^{210}Bi(β^-), ^{11}C(β^+), ^{210}Po(α) are left free. Two different approaches are used. The first approach uses Monte Carlo-generated curves in the (250–1600) keV range and accounts for external γs from the PMTs in the rightmost region, while the second approach uses analytical shapes in the (300–1250) keV range obtained after statistical subtraction of the α events (^{210}Po) as identified by pulse shape analysis. The two methods yield fully consistent results and the difference between them has been included in the systematics which now accounts to $\sim$3.5%. The final result, $46.0\pm1.5(\text{stat})^{+1.5}_{-1.6}(\text{syst})$ counts per day in 100 t, is for the first time below 5% accuracy and for the first time below the theoretical error of $\sim$ 7%. Looking directly at the ^{7}Be neutrino flux in units of 10^{9} cm^{-2} s^{-1} the flux measured by Borexino is 3.10 ± 015 or 4.84 ± 0.24 after correcting for neutrino oscillation with the best-fit parameters from global analysis [2]. The SSM-high-Z(low-Z) model foresees instead $5.00\pm0.35(4.56\pm0.32)$. Considering the high-Z model as reference, the measured-to-expected flux ratio is therefore 0.62 ± 0.05 corresponding to a survival probability of 0.5 ± 0.07, while including oscillations the ratio becomes $f(^{7}\text{Be}) = 0.97 \pm 0.09$.

Figure 5 shows the combined confidence level contours for ^{7}Be and ^{8}B measurements including the latest Borexino measurements expressed as a fraction of the reference high-Z model. Predictions from the two models with theoretical error bars are also shown. As can be seen, the present data do not allow to discriminate between the two models.

Within a global analysis, the Borexino results on ^{7}Be flux give a strong contribution in constraining the fundamental *pp* neutrino flux and reducing its error: $\Phi_{\text{pp}} = 6.06^{+0.02}_{-0.06}\cdot10^{10}$ cm^{-2} s^{-1} ($f(pp) = 1.013^{+0.003}_{-0.010}$). Figure 8b shows the impact of the Borexino measurement on the validation of the MSW-LMA model in the vacuum-dominated regime. In addition, the CNO neutrino flux can be limited to $\Phi_{\text{CNO}} < 1.3 \cdot 10^{9}$ cm^{-2} s^{-1} ($f(\text{CNO}) < 2.5$) at 95% CL. Consequently, the contribution to the SSM luminosity from CNO cycle can be limited to <1.7% at 95% CL.

2.1.3 *Day–night asymmetry.* The Borexino dataset was inspected also for a possible day–night effect. Figure 6 shows the day and night Borexino spectra, after normalizing for the exposure (385.5 live day time and 363.6 live night time). The energy region considered for the extraction of the day–night parameter is the ^{7}Be energy window (550–800 keV). The nadir angle distribution for events in this range is also shown where the exposure function used for normalization also accounts for the expected 3% seasonal modulation due to the eccentricity of Earth's orbit, which can otherwise introduce a fake day–night effect.

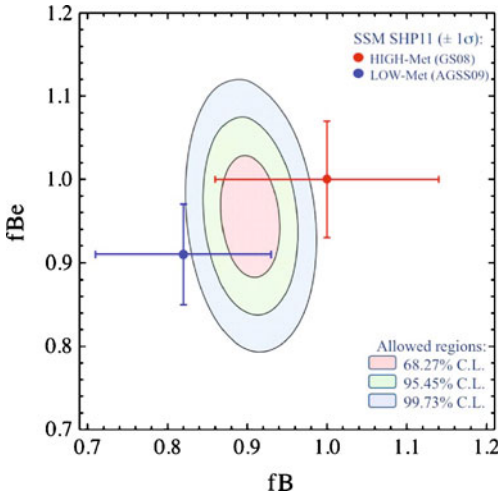

Figure 5. ^{7}Be and ^{8}B measured values as a fraction of high-Z SSM prediction, compared to the two metallicity expectations [16].

The day–night asymmetry parameter is defined as

$$A_{\mathrm{dn}} = 2\frac{R_{\mathrm{n}} - R_{\mathrm{d}}}{R_{\mathrm{n}} + R_{\mathrm{d}}} = \frac{R_{\mathrm{diff}}}{R},$$

where R_{n} and R_{d} are the ^{7}Be night and day fluxes respectively. The most effective way of extracting this parameter is to subtract the day spectrum from the night one (after normalization) and fit the resulting spectrum searching for a contribution with the ^{7}Be Compton-like shape. Figure 7a shows this procedure. The negative peak around 400 keV is not surprising: the ^{210}Po α contribution is more in the day spectrum than in the night one as the decay time is ∼200 d and data taking started at the

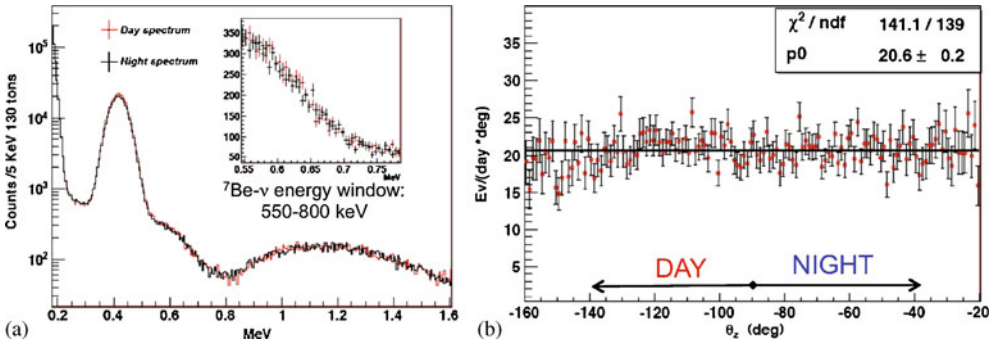

Figure 6. Borexino day and night energy spectra (**a**) and nadir angle distribution for the ^{7}Be energy region (**b**) [17].

beginning of a summer. No ^{7}Be is found in the subtracted spectrum and the resulting $A_{\rm dn} = 0.001 \pm 0.012(\text{stat}) \pm 0.007(\text{syst})$. The systematic error is given by the variation of the ^{210}Bi contamination through the dataset and by the result variation in applying the fit procedure after α statistical subtraction (as described in §2.1.2).

Figure 7b shows the impact of this measurement. When neutrino oscillations with MSW effect started to be a concrete solution to the solar neutrino problem, four minima were identified by the global analyses fits in the Δm^2_{12}, $\tan^2(\theta_{12})$ parameter plane, one of which is LMA. Among the others, the so-called LOW solution foresees a pronounced $A_{\rm dn}$ due to electron neutrino regeneration effects in the Earth matter at night. Ruling out this solution so far has required the use of KamLAND antineutrino data (see §2.5.2), while it remained allowed in solar-only global analyses although at $\Delta\chi^2 = 11.8$. Thanks to the Borexino result the LOW solution is now ruled out at $>8.5\sigma$ without the need to assume CPT invariance and the LMA best-fit point is ($\Delta^2_{12} = 5.2 \cdot 10^{-5}\,\text{eV}^2$, $\tan^2\theta_{12} = 0.46$). In addition, the hypothesis of mass-varying neutrinos [18], also implying day–night asymmetry, is ruled out at $\sim 10\sigma$.

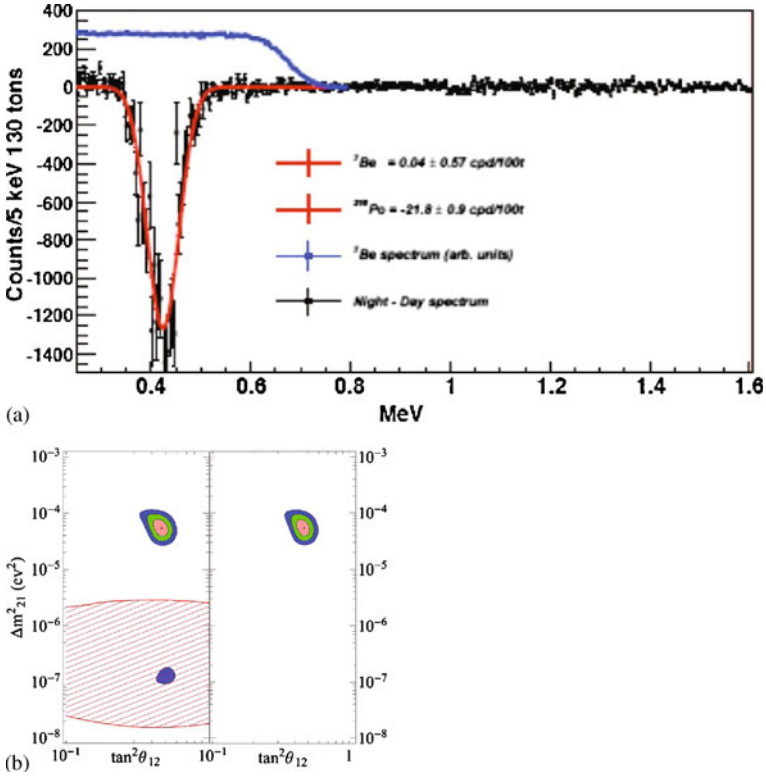

Figure 7. (**a**) Borexino night–day subtracted spectrum. (**b**) The Borexino non-observation of $A_{\rm dn}$ in the global analysis allows to reject the LOW solution at $\Delta m^2_{12} \sim 10^{-7}\text{eV}^2$ [17].

2.1.4 *^{8}B neutrino flux.* The Borexino Collaboration has also performed the measurement of the ^{8}B neutrino flux and spectrum (figure 8a). Although Borexino is small in comparison to water Cherenkov detectors for a statistically competitive measurement, the threshold reached by Borexino is the lowest ever achieved (3 MeV for the electron recoil energy). The rate measured is $0.22\pm0.04(\text{stat})\pm0.01(\text{syst})$ c/d/100 t corresponding to a flux of $\phi^{\text{ES}}_{\text{exp}} = 2.4 \pm 0.4 \pm 0.1 \cdot 10^6\,\text{cm}^{-2}\,\text{s}^{-1}$ or $\Phi^{\text{ES}}_{\text{exp}}/\Phi^{\text{ES}}_{\text{th}} = 0.88 \pm 0.19$ with respect to high-Z SSM [8]. The relevant contributions to the systematic error are: energy threshold definition ($^{+3.6\%}_{-3.2\%}$), fiducial mass ($\pm3.8\%$) and energy resolution ($^{0.0\%}_{-2.5\%}$). The analysis has also been performed by setting the energy at 5 MeV, attesting the full compatibility with the results of water Cherenkov detectors described below. The importance of performing this measurement with Borexino can be seen in figure 8b. Borexino has measured $P^{\text{vac}}_{\text{ee}}(^7\text{Be}) = 0.52^{+0.07}_{-0.06}$ and $P^{\text{matt}}_{\text{ee}}(^8\text{B}) = 0.29 \pm 0.10$ with $P^{\text{vac}}_{\text{ee}} - P^{\text{matt}}_{\text{ee}} = 0.23 \pm 0.07$. For the first time, the same detector has measured the survival probability of electron neutrinos from the Sun in the two energy regions foreseen by the MSW-LMA, the

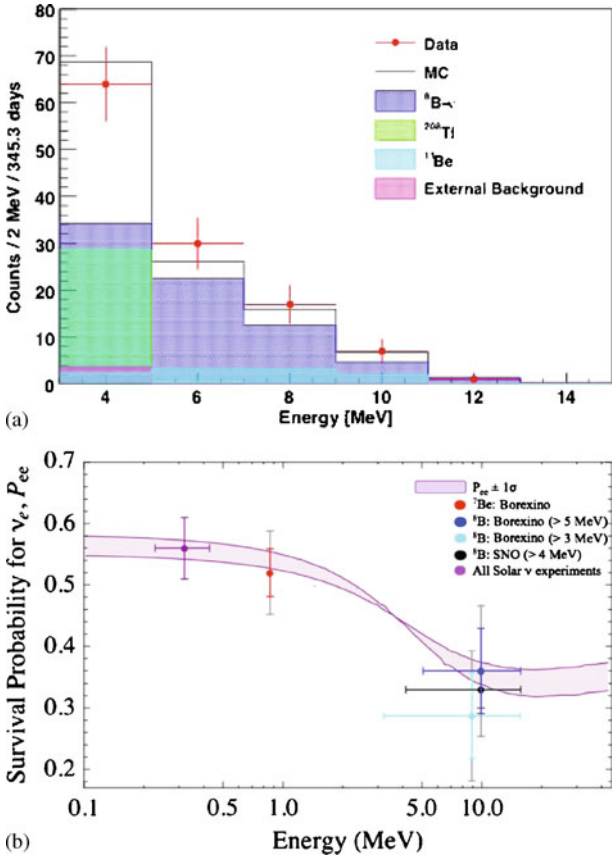

Figure 8. (**a**) Borexino ^{8}B energy spectrum. (**b**) Available measurements of P_{ee} after Borexino [19].

vacuum-dominated and the matter-enhanced regions, and obtaining different results, a striking confirmation of the model.

2.2 *Super-Kamiokande*

The Japanese Super-Kamiokande (SK) is a Water Cherenkov detector located 1000 m (2700 m w.e.) underground and since fifteen years it plays a fundamental role in most neutrino physics searches including solar, atmospheric, supernova and long baseline neutrino studies. Concerning solar neutrinos, the detector focusses on the detection of ^{8}B neutrinos via elastic scattering.

2.2.1 *The detector.* The SK [10] inner detector is a 50 kt water tank with cylindrical geometry and equipped with 11129 20″-PMTs. A fiducial volume of 22.5 kt is the standard for solar neutrino studies. An outer layer of water acts as muon detector being equipped with additional 1885 8″-PMTs.

SK started data taking in 1996 and produced brilliant results in the following years [20]. The energy threshold was 5 MeV for solar neutrinos. An accident occurred in 2001 during a maintenance operation breaking about half of the PMTs. A temporary situation called SK-II had the remaining PMTs rearranged to cover the full surface and operated with a 7 MeV threshold for ^{8}B neutrinos in years 2003–2005. In 2006 SK-III restarted with the full coverage and threshold of SK-I . Since 2008, the detector is in SK-IV phase with upgraded electronics and water plants. The current threshold is at 4.5 MeV and is targeting 4 MeV for the nearest future.

2.2.2 *Results from SK-III phase.* The SK-III phase [21] featured improved water circulation and purification system resulting in reduced radon in the FV compared to SK-I phase. The effect can be seen in the lowest energy bin (5.0, 5.5) MeV in figure 9. An additional bin is available in the spectrum at (4.5, 5.0) MeV, where solar neutrino signal is present with 4σ significance. However, the systematics for this bin is still being evaluated and is therefore not included in the fit. The SK-III spectrum shows no distortion from the shape predicted by the SSM (figure 9). The ^{8}B neutrino flux is $2.32 \pm 0.04(\text{stat}) \pm 0.05(\text{syst}) \cdot 10^6\,\text{cm}^{-2}\,\text{s}^{-1}$ to be compared with the SK-I result [20] $2.38 \pm 0.02(\text{stat}) \pm 0.08(\text{syst}) \cdot 10^6\,\text{cm}^{-2}\,\text{s}^{-1}$. As can be seen, the results are fully consistent and SK-III, although limited by a larger statistical error, features a significantly reduced systematic error thanks to the improved timing calibration of the detector.

2.2.3 *Prospects for the SK-IV phase.* At the end of the SK-III phase, the electronics has been upgraded achieving a wider dynamic range and the DAQ has been modified in view of a transition from a hardware trigger system to a software one with lower threshold possibilities. In addition, the water plants have been modified for a better control of the temperature of the water at the inlet of the detector's tank and a consequent further reduction of radon within the fiducial volume. All these improvements aim to achieve a 4 MeV threshold with half the systemic error of SK-I and test the upturn of the ^{8}B

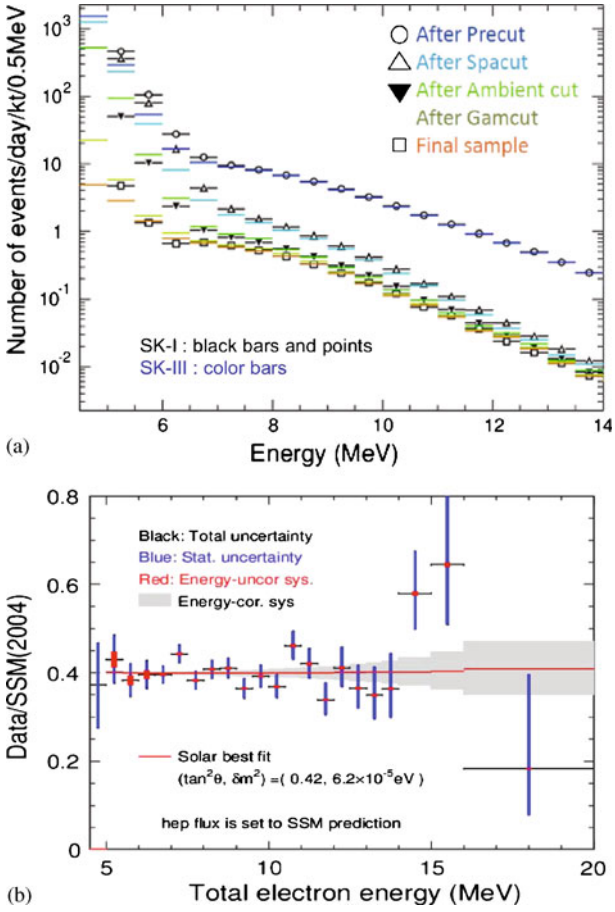

Figure 9. SK-III energy spectrum [21]. (**a**) Effect of purification in comparing with SK-I spectrum. (**b**) After being normalized to SSM predictions.

neutrino spectrum within 5 years of data taking. The expected spectrum can be seen in figure 10 [22].

2.3 *SNO*

The Sudbury Neutrino Observatory (SNO) is a 1 kt heavy water Cherenkov detector located in the Sudbury mine (Canada) at the formidable depth of 2092 m (∼6010 m w.e.) which has taken data between 1999 and 2006 giving fundamental contributions to solar neutrino physics.

2.3.1 *The detector.* The detector [11] is developed for ^{8}B solar neutrino detection and has the advantage of multiple interaction channels. Aside from neutrino–electron elastic scattering, which is diversely sensitive to neutrino flavours, heavy water allows for

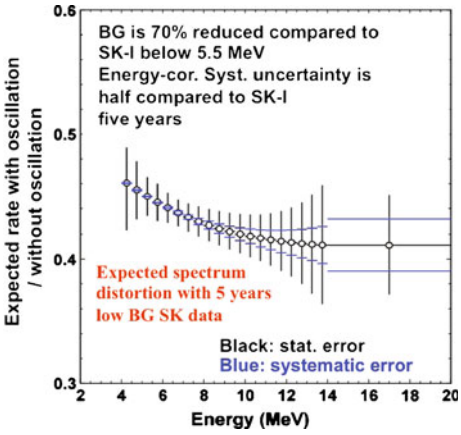

Figure 10. Expected spectrum for SK-IV phase after 5 yr of data taking [22].

charged current ($\nu_e + D \rightarrow e^- + p + p$) and neutral current ($\nu_x + D \rightarrow \nu_x + p + n$) interactions, which are sensitive to electron neutrinos only and to all neutrinos regardless of flavour, respectively. The three signals are extracted by statistical fit of the energy spectrum. In 2002 SNO measured different fluxes in the neutral and charged current interaction channels: the proof of a flavour changing mechanism operating for solar neutrinos.

The target mass of 1000 t of heavy water is contained in a 12 m-diameter acrylic vessel and is watched by 9500 PMTs allocated on an 18 m support structure for a total photocathode coverage of ∼60%. Regular water fills all volumes outside the acrylic vessel and inside the detector's cave, shielding the sensible volume from environmental radioactivity.

The data taking occurred in three successive phases. In 2001, after phase-I with pure D_2O, salt was dissolved in water to enhance the detection of neutrons from neutral current interactions. Neutron capture on ^{35}Cl in fact features a higher cross-section and a higher energy (8.6 MeV) of the γ cascade – standing better out of background – with respect to the 6.5 MeV γ from n capture on D. At the end of 2003, the salt was removed and during 2004 a set of NaI proportional counters have been deployed in strings throughout the active volume. This allowed n-capture via $n+^3\text{He} \rightarrow t + p$ reaction with a cross-section of 5330 b and the possibility of event-by-event separation. However, the phase-III, whose analysis has been finalized this year [23], did not significantly improve the brilliant results of the previous two phases [24,25].

2.4 *Low-energy threshold analysis*

The most interesting achievement of the SNO Collaboration in the last two years is the low-energy threshold analysis (LETA) [26], the complete re-analysis of the data from the first two phases lowering the energy threshold of 5.0 MeV (phase-I) or 5.5 MeV (phase-II) to 3.5 MeV with a significant gain in statistics ($\sim +70\%$). In addition, LETA is also an advanced multivariate analysis that fits the binned distributions of four variables simultaneously: the angle between the reconstructed Cherenkov track and the direction of the

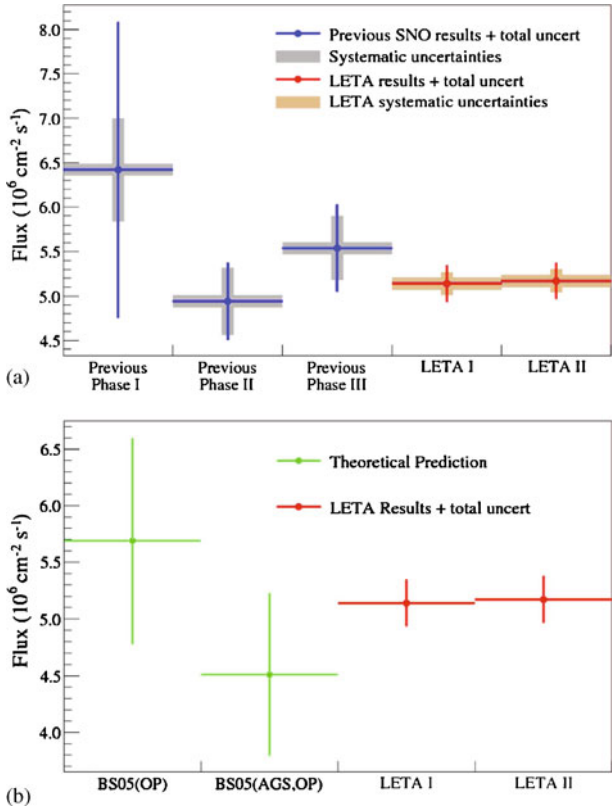

Figure 11. SNO LETA results compared to previous analyses of the three phases (**a**) and to predictions of SSM in the two metallicity cases (**b**) [26].

Sun ($\cos(\theta_{\text{Sun}})$), a shape parameter indicating the sphericity of the PMT hit distributions in the event (β_{14}), the radial distribution (R^3) and of course the reconstructed energy of the event (T_{eff}).

Figure 11 shows the striking reduction in errors (both statistical and systematical) achieved with LETA in comparison with the original analyses for the three phases and with the prediction of SSM in the two metallicity cases. As noted before (§2.1.2 and figure 5), the measured values lie between the two predictions and currently allow to disfavour neither of them. Finally, figure 12 shows the CC spectrum obtained in LETA where no clue is present of the expected upturn of the ^{8}B spectrum. Although the small statistics in the lowest energy bin does not allow to draw conclusions, this raises the interest for the upcoming measurement of SNO+ (§3.1).

2.5 *KamLAND*

KamLAND is a liquid scintillator neutrino detector located in the Kamioka mine in Japan and taking data since 2002. Its main physics targets are electron antineutrinos from

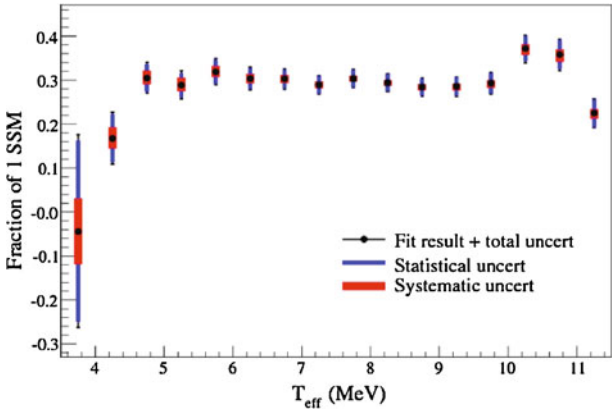

Figure 12. SNO LETA charged current interaction spectrum [26].

nuclear power reactors in Japan and Korea, ranging up to 7 MeV. The flux-weighted average baseline for KamLAND is ∼180 km which makes the oscillations directly visible in the spectrum. Under the assumption of CPT invariance, these results can be combined with solar neutrino experiments. In 2003, KamLAND's spectral distortions led to the identification of oscillations as the flavour-converting mechanism operating on solar neutrinos and of LMA as the best-fit solution in the 'solar' sector.

2.5.1 *The detector.* The primary target volume consists of 1 kt of ultrapure liquid scintillator (LS). This inner detector of LS is shielded by a 3.2-kt water-Cherenkov outer detector. Scintillation light is viewed by 1325 17″ and 554 20″ photomultiplier tubes (PMTs) providing 34% solid-angle coverage. A detailed overview of the detector is given in [12].

2.5.2 *Antineutrino spectrum from reactors.* Antineutrino detection in liquid scintillator occurs via the 'standard' Reines–Cowan technique: the antineutrino interacts via inverse beta decay $\bar{\nu}_e + p \rightarrow n + e^+$ and the signature consists of a prompt signal from positron scattering on top of the annihilation energy and a delayed signal from the neutron capture gamma (2.2 MeV on H). A typical delay between the two signals in liquid scintillator is of the order of 250 μs. So the coincidence is a powerful handle to suppress background. The process has a kinematic threshold of 1.8 MeV.

The most recent update of reactor antineutrino results from the KamLAND Collaboration is [27] and features a dataset of 2135 d live time taken from March 2002 to Apr. 2009. The spectrum can be seen in figure 13. ^{210}Po is the main radioactive background source as the α particles emitted by its decay are responsible for $^{13}C(\alpha, n)^{16}O$ reactions which simulate the coincidence signals of the antineutrino interactions. For this reason, in 2007, the LS was purified reducing the contamination of ^{210}Po by a factor of ∼20. The latest result includes ∼30% live time from the post-purification period and the background reduction is visible by comparing figure 13 with previous editions of the same plot [28]. Figure 13 also shows the spectrum as a function of $L_0/E_{\bar{\nu}_e}$ making the oscillations clearly visible.

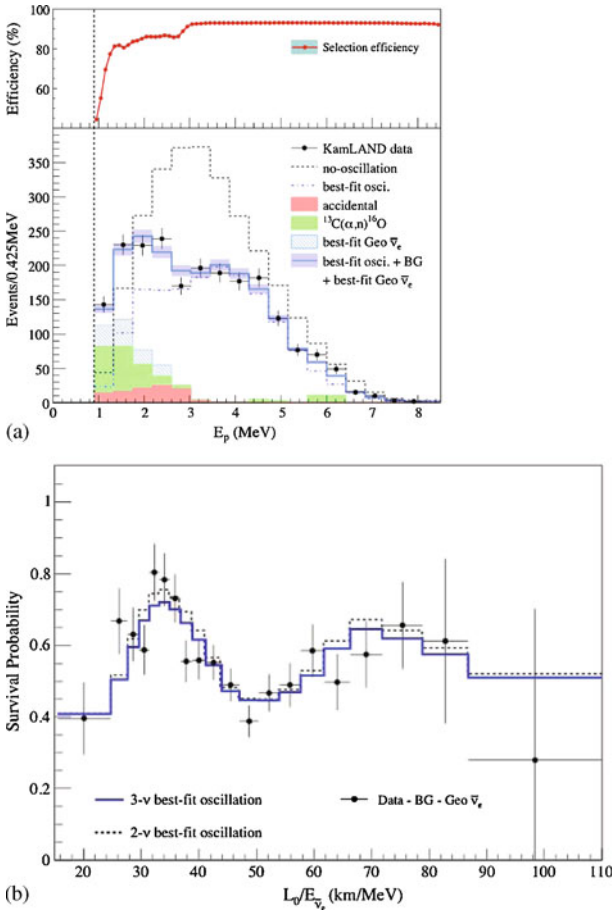

Figure 13. KamLAND reactors' data: prompt energy spectrum (**a**) and L/E distribution (**b**) [27].

2.5.3 *Global analysis.* If solar neutrino and reactors' antineutrino data are combined into a global analysis the neutrino oscillation parameters between the first two mass eigenstates can be obtained from the fit [27]. The parameter plane Δm^2_{21} vs. $\tan^2(\theta_{12})$ is shown in figure 14 in the case of 2-ν (θ_{13} fixed to 0) and 3-ν (θ_{13} left free) analysis. The best-fit points are $\tan^2\theta_{12} = 0.444^{+0.036}_{-0.030}$ and $\tan^2\theta_{12} = 0.452^{+0.035}_{-0.033}$, respectively, while $\Delta m^2_{12} = 7.50 \pm 0.20 \cdot 10^{-5}\,\mathrm{eV}^2$ in both cases. The slight tension existing between the solar-only and the KamLAND-only fit results in the 2-ν case is released in the 3-ν case and the fit returns $\sin^2(\theta_{13} = 0.02 \pm 0.016)$. This is a modest indication for a non-zero value, but it can be combined with other neutrino physics results obtaining a somewhat stronger significance (see for example [3]).

2.5.4 *Flux of ^{8}B solar neutrinos.* KamLAND recently joined the search for solar neutrinos from ^{8}B [29] using the dataset before the purification of the liquid scintillator, i.e.

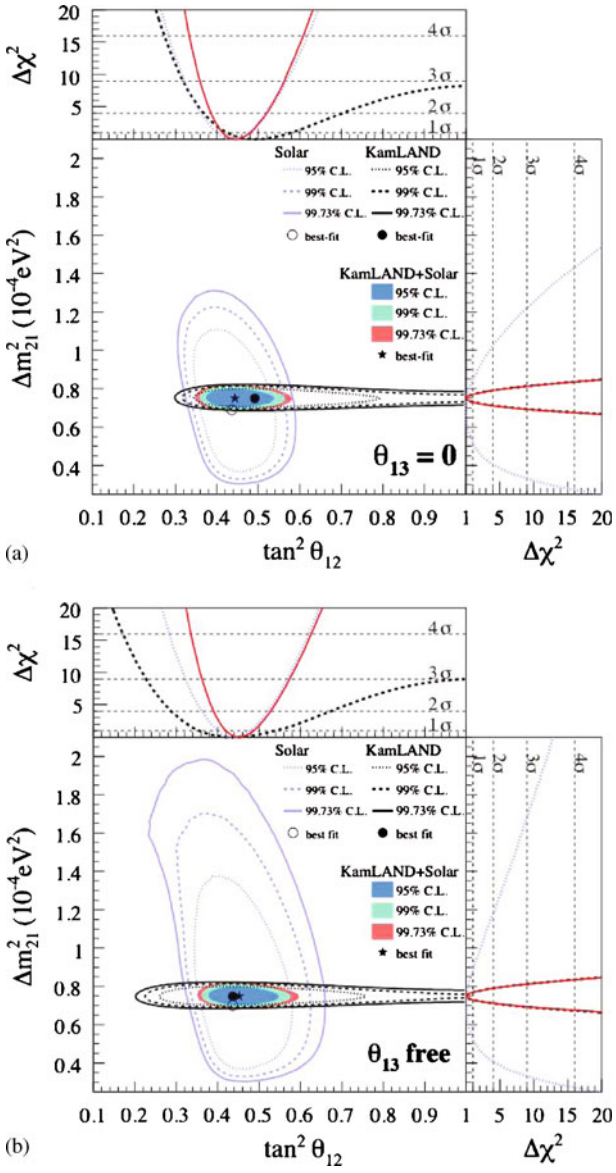

Figure 14. Δm^2_{12} vs. $\tan^2\theta_{12}$ from global analysis using solar data, KamLAND data or combining all of them. 2-ν analysis (**a**) and 3-ν analysis (**b**) are shown [27].

from Apr. 2002 to Apr. 2007 for a total of 1452 d live time. This analysis is based on neutrino–electron elastic scattering and does not benefit from the handle of the delayed coincidence with the neutron capture typical of the antineutrino inverse-beta interaction. For this analysis, a reduced fiducial volume of 176.4 m^3 and a threshold of 5.5 MeV were used. The spectrum can be seen in figure 15a. The extraction of the neutrino

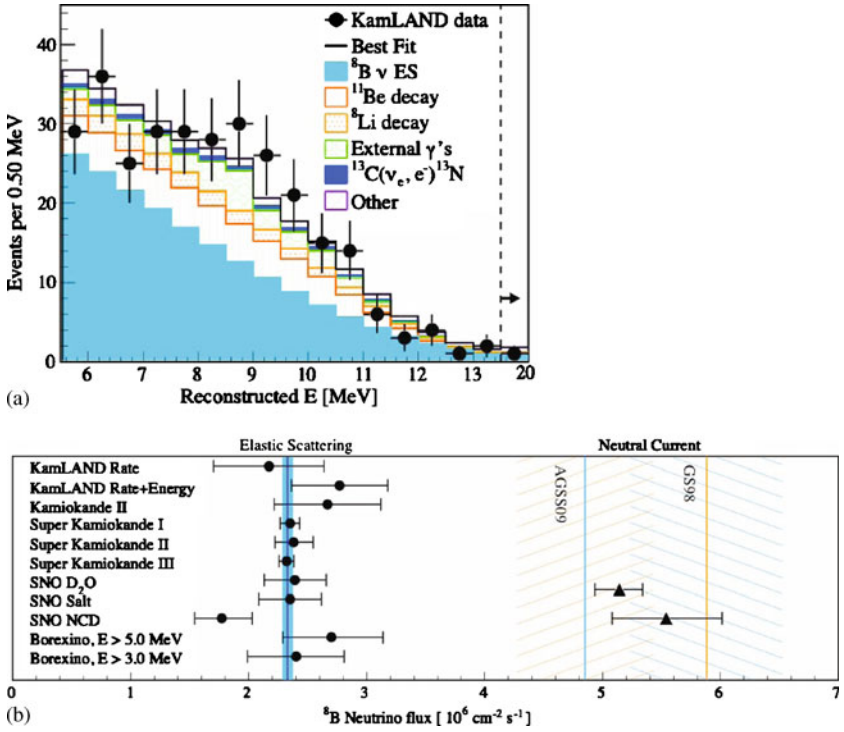

Figure 15. (**a**) KamLAND prompt energy spectrum for ^{8}B. (**b**) Comparison of all ^{8}B flux measurements [29].

flux is attempted with two approaches: a rate-only analysis and an unbinned maximum-likelihood fit of the energy spectrum. The two methods return $\Phi_{\rm ES}^{\rm Rate} = 2.17 \pm 0.26({\rm stat}) \pm 0.39({\rm syst}) \cdot 10^6\,{\rm cm}^{-2}\,{\rm s}^{-1}$ and $\Phi_{\rm ES}^{\rm Spectrum} = 2.77 \pm 0.26({\rm stat}) \pm 0.32({\rm syst}) \cdot 10^6\,{\rm cm}^{-2}\,{\rm s}^{-1}$, respectively. The main sources of systematics are the determination of background from cosmogenic radioisotopes such as ^{11}Be, ^{8}Li and ^{8}B or from external contaminants and from the determination of the detection efficiency. This result is not competitive either in terms of statistics or in terms of energy threshold with other existing measurements of the ^{8}B flux, but it represents an independent consistency check as can be seen in figure 15b where all elastic scattering ^{8}B flux measurements are compared with total errors. The weighted average is $\Phi_{\rm ES} = 2.33 \pm 0.05 \cdot 10^6\,{\rm cm}^{-2}\,{\rm s}^{-1}$ and is dominated by SK-I and SK-III results (§2.2.2).

3. Future projects in low-energy neutrino physics

The near future in solar neutrinos will see the start of the SNO+ detector, the conversion of the SNO detector into a liquid scintillator detector with a physics program that goes beyond low-energy solar neutrinos including the search for 0-ν 2β-decay by loading of the scintillator with Nd or other candidate 2β-decay isotopes [30], detection of antineutrinos

from the Earth (§4) and from reactors, neutrinos from the possible explosion of a galactic supernova and searches for nucleon decay in 'invisible' channels. Many other projects like XMASS, MOON, CLEAN and LENS are in different developmental stages.

Physicists all over the world are working since many years on next generation multipurpose detectors which are also very capable low-energy neutrino detectors. Such detectors can be megaton water Cherenkov detectors (hyper-Kamiokande, Memphys, UNO), $\sim$ 50 kt liquid scintillator detectors (LENA) or $\sim$ 5 kt liquid argon detectors (GLACIER).

Because of space constraint, we choose to briefly review here only SNO+ and LENA.

3.1 *SNO+*

The idea of the SNO+ is the conversion of the SNO detector (§2.3.1) into an organic liquid scintillator detector [31]. The density of the scintillator in the central acrylic vessel is lower than the surrounding water, which reverts the situation of the heavy water target of SNO. This posed the main construction challenge: the support structure of the vessel had to be replaced by a hold-down system. However, the first pure scintillator phase is foreseen in early 2013 after which a 2β-decay phase is scheduled for a few years before pure scintillator is returned for the detailed solar study.

In figure 16 is shown the simulated ^{8}B spectrum compared to expectations from LMA and NSI models. As it can be seen, by going below the energy range of the LETA analysis of SNO (§2.4) it will be possible to distinguish the two models. One of the dramatic advantages of this project is the very deep location, ~6010 m w.e. which virtually eliminates the problem of cosmogenic ^{11}C background in the (1, 2) MeV energy range. In SNO+ about 4000 events/yr are expected from *pep* neutrinos and a similar signal from CNO. The estimated error after three years of data taking is 5% (*pep*) and 8% (CNO) assuming the radiopurity levels obtained in Borexino (§2.1).

3.2 *LENA*

LENA is the proposed European next-generation liquid scintillator experiment [32]. Its physics program is broad, encompassing low-energy physics (supernova neutrinos from a galactic explosion but also the diffuse background; antineutrinos from reactors and from the Earth; solar neutrinos; indirect dark matter searches) and GeV physics (proton decay, atmospheric neutrinos and long-baseline neutrino oscillations if targeted by a

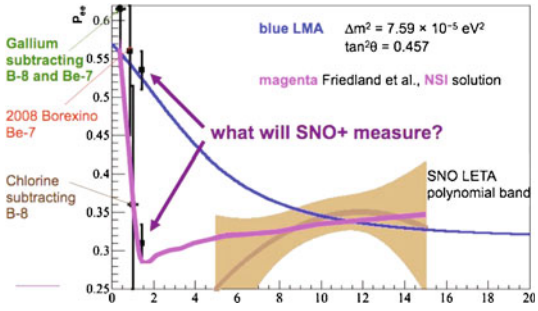

Figure 16. Projection of SNO+ sensitivity for the ^{8}B upturn [31].

beam). Concerning solar neutrinos, LENA can easily cover *pep*, CNO and ^{7}Be neutrinos to unprecedented accuracy, but also go for the fundamental *pp* neutrinos in the lowest energy region. The detector is the scale-up of present day experiments: 50 kt liquid scintillator target in a cylindrical nylon vessel (13 m radius, 100 m height) surrounded by a buffer of 20 kt inactive liquid and watched by 50000 8″ PMTs for a 30% optical coverage. A combination of water Cherenkov and streamer tube detectors would allow to track cosmic muons. The proposed location is a 4000 m w.e. deep cavern in the Phyhäsalmi mine (Finland). Research on this project started in 2005 (site studies, scintillator mixture development, PMT sealing, tank design, Monte Carlo, ...) and the collaboration based on 35 institutions from 12 countries has published the white paper in 2011 [32]. Construction time is evaluated as eight years from the time of approval.

4. Geoneutrinos

Very little is known about the Earth's interior. Neutrinos emitted by the Earth can escape freely and instantaneously and are therefore a powerful probe for the composition of the planet [33]. In particular, they can help to answer questions about the origin of the terrestrial heat (45TW), about the abundance of long-lived radioactive U and Th in the crust and in the mantle and they can be used to test the hypothesis of a natural nuclear breeder reactor in the core of the Earth. The standard geophysical model for the description of the Earth is called bulk silicate Earth (BSE) which awaits to be tested by geoneutrinos

Geoneutrinos are actually antineutrinos emitted within the decay chains of long-lived radioisotopes, namely ^{238}U, ^{232}Th, and in the decay of ^{40}K. The ^{238}U chain emits neutrinos up to $\sim$3.3 MeV maximum energy, while ^{232}Th only reaches 2.2 MeV and ^{40}K emits only $\bar{\nu}$ below the kinematic threshold for inverse beta detection (see §2.5.2 for antineutrino detection in liquid scintillator detectors). The spectrum can be seen in figure 17a. The Th/U$\simeq$3.9 ratio is supposed to be fixed by the analysis of chondrites, meteorites that share their origin with the solar system. These elements are present in the crust although with unknown abundance, while it is not at all clear whether they are there in the mantle as well or not.

The oceanic crust is thinner ($<$10 km) than the continental crust ($>$30 km) and a detector located in the middle of a continent would see a higher signal than the one located in a costal area and definitely higher than one in the middle of the ocean. At the same time, a contribution from the mantle would be uniform. Consequently, measurements performed by detectors 'seeing' different crustal contributions can be combined to disentangle roles of the mantle and the crust. On the other end, the main background source for detection of geoneutrinos are antineutrinos from nuclear power production (§2.5.2). So areas with high density of plants are not good candidate locations. In figure 17b the S/B ratio of the existing and planned experimental sites can be seen.

4.1 *KamLAND*

The KamLAND experiment (§2.5) lies at the edge between continental and oceanic crust and in a region highly populated with nuclear power plants. The S/B ratio is $\sim$0.2 without considering additional sources of background. Nevertheless, they have analysed a 4126

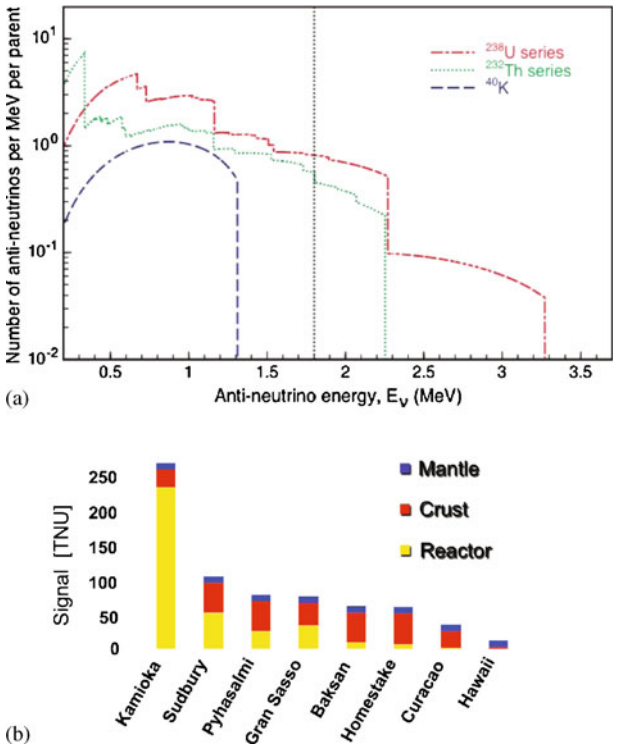

Figure 17. (**a**) Energy spectrum of geoneutrinos; the dashed vertical line shows the threshold for inverse β decay. (**b**) Expected signal and background at current and planned sites for geoneutrino detectors [33].

t-y dataset for geoneutrinos [34] and found 841 candidate events in the (0.9, 2.6) MeV energy range. Backgrounds have been evaluated for the following amounts: reactor $\bar{\nu}_e$ (484.7±26.5), $^{13}C(\alpha, n)^{16}O$ reactions (165.3±18.2), accidental coincidences (77.4±0.1), cosmogenic ^{9}Li(2.0±0.1) and atmospheric ν plus fast neutrons (<2.8) for a total of 729.4±32.3. The hypothesis of no geoneutrinos is therefore excluded from a rate-only test at 99.55% CL. The energy spectrum is shown in figure 18 along with backgrounds and after their subtraction it is compared with expected signal from BSE. The number of geoneutrinos from a fit to the spectrum is 106^{+29}_{-28} assuming the fixed ratio U/Th=3.9. The $\Delta\chi^2$ profile for the geoneutrino component is also shown in figure 18. The resulting flux is $\Phi_{\text{geo}} = 4.3^{+1.2}_{-1.1} \cdot 10^6\,\text{cm}^{-2}\,\text{s}^{-1}$.

4.2 *Borexino*

Although smaller in size, Borexino is located on continental crust and about 800 km from the nearest nuclear power plants. Its S/B ratio of ∼0.4 is therefore more favourable than KamLAND's. In addition, the much lower contamination of ^{210}Po in the scintillator (the

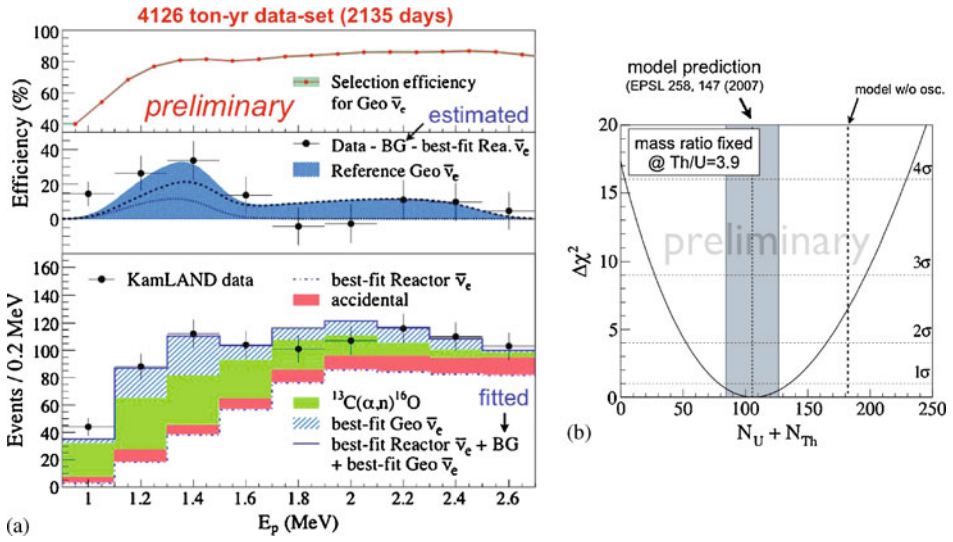

Figure 18. KamLAND prompt energy spectrum for geoneutrinos (**a**) and the $\Delta\chi^2$ profile of the fit result (**b**) [34].

α emitter responsible for the $^{13}C(\alpha, n)^{16}O$ reactions) and the thicker rock coverage make Borexino almost free from non-reactor's backgrounds. The 252.6 t-y dataset has been analysed [35] finding 21 antineutrino candidates. A fit to the energy spectrum (figure 19) assigns ∼10 events to geoneutrinos and ∼11 events to reactor $\bar{\nu}$ for a resulting flux of $\Phi_{geo} = 7.3^{+3.0}_{-2.4} \cdot 10^6\,cm^{-2}\,s^{-1}$. The hypothesis of no geoneutrinos is rejected at 99.997% CL (4.2σ). Also the hypothesis of a georeactor at the Earth's centre with more than 3 TW power is disfavoured at 95% CL.

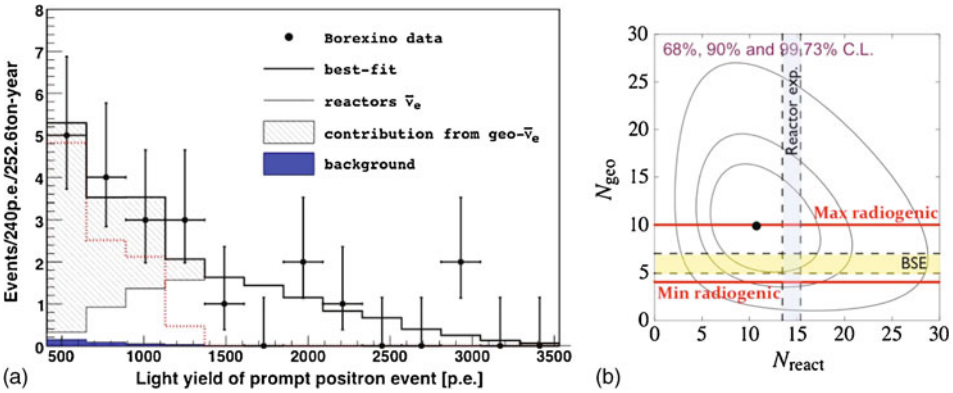

Figure 19. Borexino prompt $\bar{\nu}$ energy spectrum (**a**) and how the fit assigns the candidates to reactors and geoneutrinos (**b**) [35].

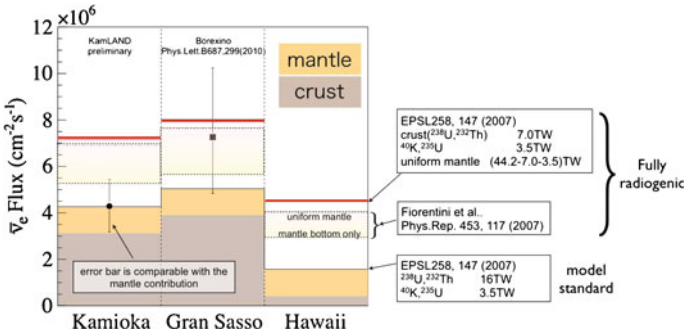

Figure 20. Comparison between existing measurements of geoneutrinos and predictions from BSE and fully-radiogenic models [34].

4.3 *Comparing data and model*

Figure 20 shows the fluxes measured by KamLAND and Borexino compared to geoneutrino expectations from BSE at Kamioka mine and Gran Sasso, respectively. Contribution from the mantle and the crust are evidenced. The BSE model assigns about 20 TW of the terrestrial heat to radioactive decays. However, alternative 'fully radiogenic' models can ascribe all 45 TW to this source. KamLAND result seems to favour the BSE model, while Borexino result is in a better agreement with fully radiogenic models, although the present errors do not allow one to draw conclusions yet. The third column in figure 20 shows predictions for a proposed experiment (Hano-hano [36]) to be performed by sinking a liquid scintillator detector deep in the ocean. The experiment is proposed to take place on a custom ship located at the Hawaii islands, where the small crustal contribution would allow us to measure geoneutrinos from the mantle. The upcoming SNO+ experiment (§3.1), thanks to its favourable location, can count on a $S/B \sim 1.2$ and is therefore expected to play a major role in the coming years also in geoneutrino physics.

5. Conclusions

Low-energy solar neutrino experiments give fundamental contributions in answering the open questions in solar astrophysics and in understanding the mechanism of neutrino oscillations. We have reviewed the recent progresses from Borexino: the experimental error on ^{7}Be neutrinos has been reduced to 5% and no day/night asymmetry has been observed; ^{8}B flux has been measured with the lowest threshold of 3 MeV. The neutrino oscillation mechanism with MSW effect and the LMA solution has been therefore validated both in the low-energy vacuum-dominated regime and in the high-energy matter-enhanced regime, but a consistent effort is now put into the transition region ((1, 3) MeV) where *pep* neutrinos are to be found and where the NSI model would show a different survival probability shape. To probe the transition region, all experiments are trying to lower the detection threshold of ^{8}B neutrinos. We have reviewed the evolution of Super-Kamiokande leading measurement through SK-III and SK-IV phases, we have

reported about the powerful low-energy threshold analysis from SNO that goes down to 3.5 MeV with large statistics and about the consistency checks performed by KamLAND. We have reviewed the latest reactor antineutrino data release from KamLAND and the global analysis combining them to solar data. Among upcoming projects we have selected SNO+ as having great potentiality in lowering the ^{8}B threshold to 1 MeV and in detecting *pep* and the so far undetected CNO neutrinos. Among next-generation experiments proposed, we have indicated that LENA has the best potential in solar neutrino physics.

At the same time Borexino and KamLAND have measured the flux of antineutrinos produced by radioactive decays in the Earth's crust and possibly in the mantle. Such measurements are ideal probes of the geophysical models such as BSE and more accurate measurements are awaited to understand how the terrestrial heat is generated and to shed light into the mystery of the Earth's composition.

References

[1] L Wolfenstein, *Phys. Rev.* **D17**, 2369 (1978)
S P Mikheev and A Yu Smirnov, *Sov. J. Nucl. Phys.* **42**, 913 (1985)
[2] Particle Data Group: K Nakamura *et al*, *J. Phys.* **G37**, 075021 (2010)
[3] T Schwetz, *These proceedings*
[4] A M Serenelli, W C Haxton and C Pena-Garay, *Astrophys. J.* **743**, 24 (2011)
[5] A Friedland *et al*, *Phys. Lett.* **B597**, 347 (2004)
[5a] These experiments had no spectroscopical capabilities. Instead, their signal was composed of undistinguished interactions of all neutrinos above their detection threshold of 233 keV. Accurately subtracting the ^{7}Be and other species leaves the *pp* flux emerge
[6] N Grevesse and J Sauval, *Sp. Sc. Rev.* **85**, 161 (1998)
[7] M Asplund, N Grevesse, J Sauval and P Scott, *Ann. Rev. Astr. Astrophys.* **47**, 481 (2009)
[8] A Serenelli, S Basu, J W Ferguson and M Asplund, *Astrophys. J.* **705**, L123 (2009)
[9] Borexino Collaboration: G Alimonti *et al*, *Nucl. Instrum. Methods* **A600**, 568 (2009)
[10] Super-Kamiokande Collaboration: Y Fukuda *et al*, *Nucl. Instrum. Methods* **A501**, 418 (2003)
[11] SNO Collaboration: J Boger *et al*, *Nucl. Instrum. Methods* **A449**, 172 (2000)
[12] KamLAND Collaboration: S Abe *et al*, *Phys. Rev.* **C81**, 025807 (2010)
[13] Borexino Collaboration: G Bellini *et al*, *J. Instrum.* **6**, P05005 (2011)
[14] Borexino Collaboration: C Arpesella *et al*, *Phys. Rev. Lett.* **101**, 091302 (2008)
[15] Borexino Collaboration: G Bellini *et al*, *Phys. Rev. Lett.* **107**, 141302 (2011)
[16] Borexino Collaboration: B Caccianiga, *Proc. of 12th TAUP Conference* (Munich, 2011)
[17] Borexino Collaboration: G Bellini *et al*, *Phys. Lett.* **B707**, 22 (2012), arXiv:1104.2150
[18] P C de Holanda, *J. Cosmol. Astropart. Phys.* **0907**, 024 (2009)
[19] Borexino Collaboration: G Bellini *et al*, *Phys. Rev.* **D82**, 033006 (2010)
[20] Super-Kamiokande Collaboration: J Hosaka *et al*, *Phys. Rev.* **D73**, 112001 (2006)
[21] Super-Kamiokande Collaboration: K Abe *et al*, *Phys. Rev.* **D83**, 052010 (2011)
[22] S Yamada for the Super-Kamiokande Collaboration, talk at Physun (2010), http://physun2010.mi.infn.it/PHYSUN_yamada.pdf
[23] SNO Collaboration: B Aharmin *et al*, *Phys. Rev.* C (2011) (submitted), arXiv:1107.2901
[24] SNO Collaboration: B Aharmin *et al*, *Phys. Rev.* **C75**, 045502 (2007)
[25] SNO Collaboration: B Aharmin *et al*, *Phys. Rev.* **C72**, 055502 (2005)
[26] SNO Collaboration: B Aharmin *et al*, *Phys. Rev.* **C81**, 055504 (2010)
[27] KamLAND Collaboration: S Abe *et al*, *Phys. Rev.* **D83**, 052002 (2011)

[28] KamLAND Collaboration: T Araki *et al*, *Phys. Rev. Lett.* **94**, 081801 (2005)
[29] KamLAND Collaboration: S Abe *et al*, *Phys. Rev.* **C84**, 035804 (2011)
[30] K Zuber, *These proceedings*
[31] S Biller, talk at *XIV Neutrino Telescopes* (Venice, Italy, 2011)
[32] LENA Collaboration: M Wurm *et al*, *Astropart. Phys.* **35**, 685 (2012), arXiv:1104.5620
[33] G Fiorentini, M Lissia and F Mantovani, *Phys. Rep.* **453**, 117 (2007)
[34] I Shimizu for the KamLAND Collaboration, talk at *Neutrino Geosience* (2010), http://geoscience.lngs.infn.it/Program/Pdf_presentations/Shimizu.pdf
[35] Borexino Collaboration: G Bellini *et al*, *Phys. Lett.* **B687**, 299 (2010)
[36] S T Dye *et al*, *Earth Moon Planets* **99**, 241 (2006)